

# TESTING THE MILLISECOND PULSAR SCENARIO OF THE GALACTIC CENTER GAMMA-RAY EXCESS WITH VERY HIGH ENERGY GAMMA-RAYS

QIANG YUAN<sup>1,2</sup> AND KUNIHITO IOKA<sup>2,3</sup>

<sup>1</sup>Department of Astronomy, University of Massachusetts, Amherst, MA 01002, USA

<sup>2</sup>Theory Center, Institute of Particle and Nuclear Studies, KEK, Tsukuba 305-0801, Japan

<sup>3</sup>Department of Particle and Nuclear Physics, the Graduate University for Advanced Studies (Sokendai), Tsukuba 305-0801, Japan

*Draft version January 26, 2022*

## ABSTRACT

The recent analyses of the Fermi Large Area Telescope data show an extended GeV  $\gamma$ -ray excess on top of the expected diffuse background in the Galactic center region, which can be explained with annihilating dark matter or a population of millisecond pulsars (MSPs). We propose to observe the very high energy  $\gamma$ -rays for distinguishing the MSP scenario from the dark matter scenario. The GeV  $\gamma$ -ray MSPs should release most energy to the relativistic  $e^\pm$  wind, which will diffuse in the Galaxy and radiate TeV  $\gamma$ -rays through inverse Compton scattering and bremsstrahlung processes. By calculating the spectrum and spatial distribution, we show that such emission is detectable with the next generation very high energy  $\gamma$ -ray observatory, the Cherenkov Telescope Array (CTA), under reasonable model parameters. It is essential to search for the multi-wavelength counterparts to the GeV  $\gamma$ -ray excess for solving this mystery in the high energy universe.

*Subject headings:* radiation mechanisms: nonthermal — pulsars: general — cosmic rays — gamma rays: theory

## 1. INTRODUCTION

The observations of high energy  $\gamma$ -rays from the Galactic center (GC) have revealed very interesting features at different scales. The atmospheric imaging Cherenkov telescope array, High Energy Stereoscopic System (HESS), has discovered a point-like source<sup>1</sup> which may be originated from the central supermassive black hole (Aharonian et al. 2004) as well as an extended source from the ridge which could be explained through the interaction of a fresh cosmic ray (CR) source with the interstellar medium (ISM) (Aharonian et al. 2006). The analyses of the data from the space-borne  $\gamma$ -ray detector, Fermi Large Area Telescope (Fermi-LAT), have also revealed the corresponding point-like (Chernyakova et al. 2011) and ridge emission (Yusef-Zadeh et al. 2013; Macias & Gordon 2014). Moreover, an even more extended, circular  $\gamma$ -ray excess on top of the central point and ridge emission has been identified in the Fermi-LAT data by quite a few groups (Goodenough & Hooper 2009; Vitale et al. 2009; Hooper & Goodenough 2011; Boyarsky et al. 2011; Abazajian & Kaplinghat 2012; Gordon & Macías 2013; Hooper & Slatyer 2013; Huang et al. 2013; Abazajian et al. 2014a; Daylan et al. 2014; Zhou et al. 2014; Calore et al. 2014a; Fermi-LAT collaboration 2014). Finally, the bubble structure on the Galactic scale has also been shown in the Fermi-LAT data (Dobler et al. 2010; Su et al. 2010; Su & Finkbeiner 2012; Yang et al. 2014; Ackermann et al. 2014). Those multi-scale, wide-band features have very interesting implications of the GC activity and stellar history (Crocker et al. 2011; Crocker 2012).

The circularly symmetric  $\gamma$ -ray excess is of special interest since it may connect with the emission from dark matter (DM) annihilation in the GC (Goodenough & Hooper 2009; Hooper & Goodenough 2011; Abazajian & Kaplinghat 2012; Gordon & Macías 2013; Hagiwara et al. 2014; Abazajian et al. 2014a; Daylan et al. 2014). The de-projected

spatial distribution of the  $\gamma$ -ray source follows approximately  $\theta^{-2.4}$ , with  $\theta$  the angle away from the GC, which seems to be consistent with the DM annihilation with a generalized Navarro-Frenk-White (gNFW, Navarro et al. 1997; Zhao 1996) density profile. The energy spectrum peaks at several GeV, and can be well fitted with the scenario of DM annihilation into a pair of quarks or  $\tau$  leptons with mass of DM particles 10s GeV (Hooper & Goodenough 2011; Abazajian & Kaplinghat 2012; Gordon & Macías 2013). Nevertheless, the astrophysical scenarios such as a population of unresolved millisecond pulsars<sup>2</sup> (MSPs, Wang et al. 2005; Abazajian 2011; Mirabal 2013; Yuan & Zhang 2014; Calore et al. 2014b), as well as the CR interactions in the GC may also account for this  $\gamma$ -ray excess (Carlson & Profumo 2014; Petrović et al. 2014). On the other hand, other observations of CRs and radio emission seem to have tension with the DM annihilation scenario, although they still suffer from uncertainties (Bringmann et al. 2014; Cirelli et al. 2014; Hooper et al. 2014). The origin of the  $\gamma$ -ray excess is still in debate, and we may need future, multi-wavelength observations to test different models.

The MSP scenario is favored for several reasons. The spectrum of the GeV  $\gamma$ -ray excess is very similar to those observed for MSPs (Abdo et al. 2013) and for some of the globular clusters (Abdo et al. 2010). The MSPs are old enough to extend to relatively large scale which can possibly explain the large extension of the GeV  $\gamma$ -ray excess (Daylan et al. 2014). The observed distribution of the Galactic low mass X-ray binaries (Revnivtsev et al. 2008), the progenitors of MSPs, just follows the  $\theta^{-2.4}$  profile as observed for the  $\gamma$ -ray signal (Yuan & Zhang 2014). If there is a population of unresolved  $\gamma$ -ray MSPs in the Galactic bulge to contribute to the  $\gamma$ -ray excess, one would naturally expect that a portion (probably most) of the spin-down energy should be carried by the relativistic  $e^\pm$  winds from those pulsars. Such wind  $e^\pm$  may further be accelerated up to very high ener-

<sup>1</sup> See Kosack et al. (2004) for an earlier potential detection of it with significance  $\sim 3.7\sigma$  by Whipple.

<sup>2</sup> See, however, Hooper et al. (2013) and Cholis et al. (2014).

gies (VHE; TeV energies) in the shocks produced by the pulsar winds (Bednarek & Sitarek 2007; Bednarek & Sobczak 2013). Then these leptons will diffuse into the ISM in the Galaxy, and radiate through inverse Compton scattering (ICS), bremsstrahlung and synchrotron emission. Since the  $e^\pm$  wind generally dominates the energy budget over the GeV  $\gamma$ -rays from pulsars, we should investigate such emission from  $e^\pm$ . The future observations of the VHE  $\gamma$ -rays from the GC region by e.g., the Cherenkov Telescope Array (CTA, Acharya et al. 2013), could test the MSP scenario of the Fermi GeV  $\gamma$ -ray excess, and may distinguish it from the DM scenario (Lacroix et al. 2014; Abazajian et al. 2014b).

In this work we explore the VHE  $\gamma$ -ray emission associated with the relativistic  $e^\pm$  winds from the GC MSPs, using the Fermi  $\gamma$ -ray excess as a normalization of the MSP population. In Sec. 2 we briefly describe the  $e^\pm$  production model of MSPs. The major results of the VHE  $\gamma$ -ray emission from the MSP  $e^\pm$  and the detectability with CTA will be given in Sec. 3. We conclude and discuss the results in Sec. 4.

## 2. $E^\pm$ FROM MSPS

It has been well established that the rotation-powered pulsars release most of their rotational energy as a relativistic wind of magnetized  $e^\pm$  plasma from the magnetosphere (Rees & Gunn 1974). The interaction of such a wind with the ISM will then form a shock, which can also accelerate the  $e^\pm$  to VHE. The synchrotron or ICS emission from these  $e^\pm$  form the so-called pulsar wind nebula (PWN).

Assuming that the pulsar spin-down power is predominantly carried away by the kinetic energy of the wind particles, one has (Kennel & Coroniti 1984a,b)

$$L_{\text{sd}} = \gamma_w \dot{N}_{\text{GJ}} m_e c^2 \kappa (1 + \sigma) / f_{e^\pm}, \quad (1)$$

where  $L_{\text{sd}}$  is the spin-down power of the pulsar,  $\gamma_w$  is the Lorentz factor of the wind particles,  $\dot{N}_{\text{GJ}}$  is the Goldreich-Julian current (Goldreich & Julian 1969),  $m_e$  is the electron mass,  $c$  is the speed of light,  $\kappa$  is the  $e^\pm$  pair multiplicity,  $\sigma$  is the magnetization parameter (the ratio of the Poynting flux to the kinetic energy flux), and  $f_{e^\pm}$  is the relative energy fraction carried by  $e^\pm$  particles. For typical parameters of MSPs, the Lorentz factor of the wind particles can be derived as (Cheng et al. 2006, 2010)

$$\gamma_w = 4 \times 10^5 (f_{e^\pm} / \kappa_3) L_{34}^{1/2}, \quad (2)$$

where  $L_{34}$  is the spin-down power in unit of  $10^{34}$  erg s $^{-1}$ , and  $\kappa_3 = \kappa / 10^3$ . The spin-down power carried away by the  $e^\pm$  pairs is simply  $L_{e^\pm} = f_{e^\pm} L_{\text{sd}}$ . Typically we will have  $f_{e^\pm} \approx 1$ . The energy distribution of the wind  $e^\pm$  could be relativistic Maxwellian (Aharonian et al. 2012). For simplicity we adopt monochromatic injection of the wind  $e^\pm$  for the case without considering the possible acceleration or cooling in the PWN (see below).

The pulsar winds may further be accelerated in the shock region if exists (Bednarek & Sitarek 2007; Bednarek & Sobczak 2013). In the GC stellar cluster, the maximum achievable energy of the  $e^\pm$  can be as high as 50 TeV (Bednarek & Sobczak 2013). The fraction of  $e^\pm$  which are accelerated, and the final spectrum of the accelerated  $e^\pm$  are not clear. We may simply assume a power-law spectrum with an exponential cutoff at the maximum energy (Bednarek & Sobczak 2013). The total power of the accelerated  $e^\pm$  can be absorbed in the efficiency  $f_{e^\pm}$ .

Finally, the  $e^\pm$  may radiate and lose energy inside the PWN. For the young pulsar (e.g., Crab), most of the spin-down energy is released through synchrotron radiation in the nebula. However, it may not be the case for the MSPs since they are generally old and their PWNe are so extended that the magnetic field is weak (Kashiyama et al. 2011; Kisaka & Kawanaka 2012). Therefore we assume a fraction of the  $e^\pm$  can escape away from the PWN into the ISM of the Galaxy, and absorb this fraction in the efficiency  $f_{e^\pm}$ .

As for the spatial distribution of the  $e^\pm$  injection, we adopt the result inferred from the  $\gamma$ -ray excess, i.e., a spherical power-law distribution  $r^{-2.4}$  which extends to  $\sim 1.5$  kpc ( $\sim 10^\circ$ ) (Hooper & Goodenough 2011; Abazajian & Kaplinghat 2012; Gordon & Macías 2013; Daylan et al. 2014). The  $\gamma$ -ray emission ( $e^\pm$  source) may extend to even large scales (Daylan et al. 2014; Zhou et al. 2014). However, it will not significantly affect the results of the current study which focuses on the GC region.

In summary, we will discuss either monochromatic or power-law injection of  $e^\pm$  in the extended region around the GC, which represent the scenario without or with acceleration in the pulsar wind shocks, respectively. The canonical model parameters of the  $e^\pm$  are tabulated in Table 1. Furthermore, we will assume that the typical  $\gamma$ -ray efficiency with respect to the spin-down power is 0.1 (Abdo et al. 2013). Thus we have  $L_{e^\pm} = f_{e^\pm} L_{\text{sd}} = 10 f_{e^\pm} L_\gamma$ .

TABLE 1  
INJECTION  $e^\pm$  PARAMETERS: INJECTION ENERGY  $E_{\text{inj}}$  FOR THE MONOCHROMATIC CASE, SPECTRAL INDEX  $\alpha$  AND CUTOFF ENERGY  $E_{\text{max}}$  FOR THE POWER-LAW CASE, AND THE  $e^\pm$  ENERGY FRACTION OF THE SPINDOWN POWER  $f_{e^\pm}$ .

Spectrum	$E_{\text{inj}}$ (GeV)	$\alpha$	$E_{\text{max}}$ (GeV)	$f_{e^\pm}$
$\delta(E - E_{\text{inj}})$	200	...	...	0.9 or 0.1
$\delta(E - E_{\text{inj}})$	20	...	...	0.9 or 0.1
$E^{-\alpha} \exp(-E/E_{\text{max}})$	...	2.0	$5 \times 10^4$	0.9 or 0.1

## 3. VHE $\gamma$ -RAY EMISSION OF GC MSPS

Given the above source injection of relativistic  $e^\pm$ , we use GALPROP<sup>3</sup> numerical tool (Strong & Moskalenko 1998; Moskalenko & Strong 1998) to calculate the propagation of the  $e^\pm$  as well as the secondary  $\gamma$ -ray emission through ICS and bremsstrahlung. We use the default magnetic field in GALPROP, which is about 5  $\mu$ G in the GC. Thus the synchrotron energy loss of the  $e^\pm$  is less important compared with the ICS energy loss given the very strong optical radiation in the GC ( $\sim 10$  eV cm $^{-3}$ ; Moskalenko et al. 2006). The diffusion with reacceleration configuration of the propagation model is adopted. Three groups of the propagation parameters are adopted with the characteristic height of the propagation halo,  $z_h$ , varying from 2 to 10 kpc (Ackermann et al. 2012). Such a range will largely cover the uncertainties of the propagation parameters (Trotta et al. 2011; Jin et al. 2014). The propagation parameters are given in Table 2.

The calculated ICS and bremsstrahlung spectra from the propagated  $e^\pm$  produced by the MSPs in  $7^\circ \times 7^\circ$  region around the GC are shown in Figs. 1 and 2, for the monochromatic injection and the power-law injection, respectively. The Fermi-LAT data of the  $\gamma$ -ray excess (Gordon & Macías 2013), together with the direct  $\gamma$ -ray emission expected from a pop-

<sup>3</sup> <http://galprop.stanford.edu/>

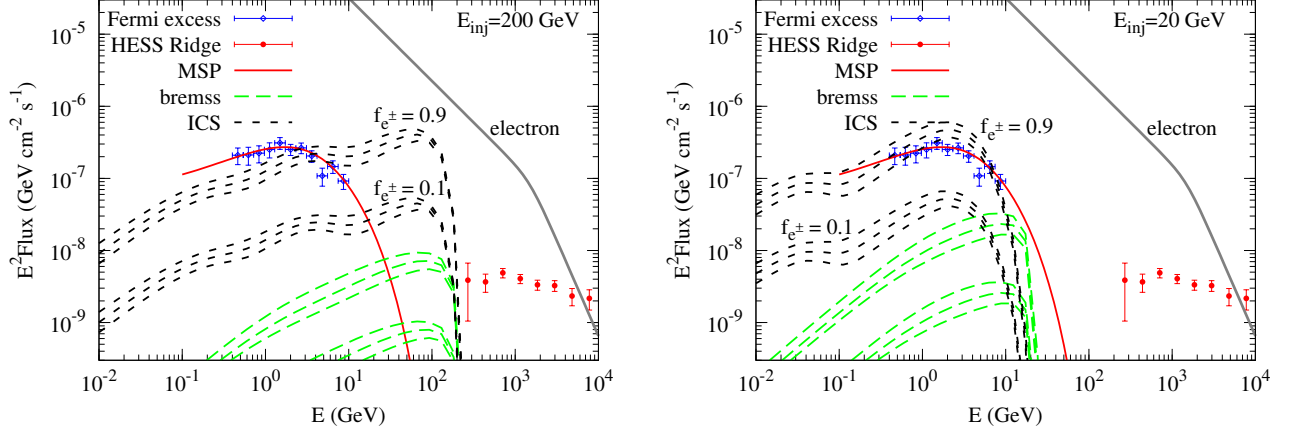


FIG. 1.— Expected ICS (short dashed) and bremsstrahlung (long dashed) emission from the wind  $e^\pm$  of the MSPs in the bulge, compared with the direct  $\gamma$ -ray emission from MSPs (solid) and the Fermi-LAT data of the excess (Gordon & Macías 2013). The three lines of the ICS and bremsstrahlung groups represent three different settings of propagation parameters in Table 2, with  $z_h$  increasing from top to bottom. The  $\gamma$ -ray emission in  $7^\circ \times 7^\circ$  region around the GC is integrated. The left panel is for the monochromatic injection of  $e^\pm$  with  $E_{\text{inj}} = 200$  GeV, and the right panel is for  $E_{\text{inj}} = 20$  GeV. As a comparison, the gray line shows the fluxes of the CR  $e^\pm$  integrated in the same sky region according to the AMS-02 (Aguilar et al. 2014) and HESS (Aharonian et al. 2008) data. Also shown the HESS observations of the diffuse emission from the GC ridge integrated in the region  $|l| < 0^\circ.8$ ,  $|b| < 0^\circ.3$  (Aharonian et al. 2006).

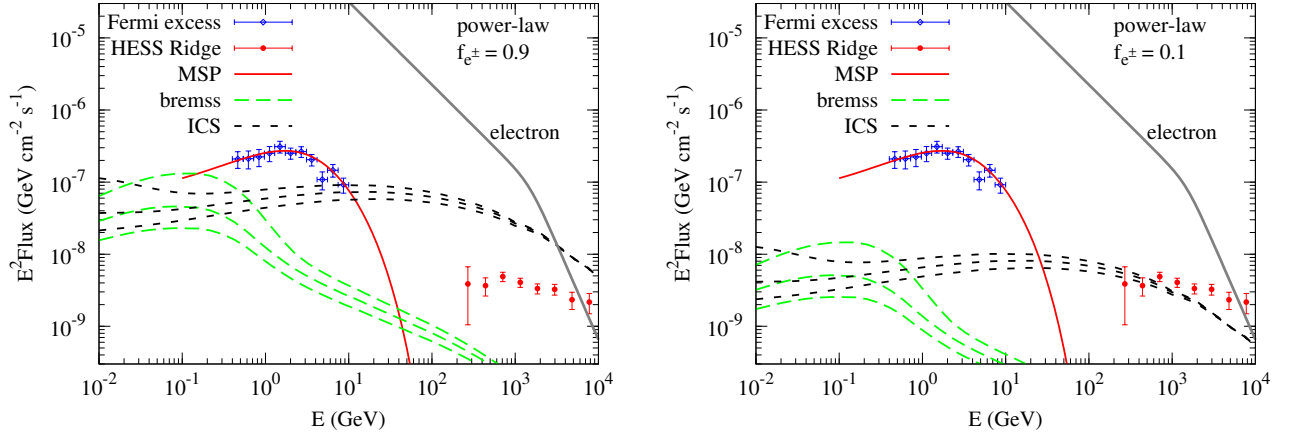


FIG. 2.— Same as Fig. 1 but for the exponential cutoff power-law injection of the  $e^\pm$ . The left panel is for  $f_{e^\pm} = 0.9$  and the right panel is for  $f_{e^\pm} = 0.1$ .

TABLE 2

COSMIC RAY PROPAGATION PARAMETERS. COLUMNS FROM LEFT TO RIGHT ARE THE DIFFUSION COEFFICIENT  $D_0$  AT THE REFERENCE RIGIDITY  $R = 4$  GV, HEIGHT OF THE PROPAGATION HALO  $z_h$ , ALFVEN SPEED  $v_A$  WHICH CHARACTERIZES THE REACCELERATION, AND POWER-LAW INDEX  $\delta$  OF THE RIGIDITY DEPENDENCE OF THE DIFFUSION COEFFICIENT.

	$D_0$ ( $10^{28} \text{ cm}^2 \text{ s}^{-1}$ )	$z_h$ (kpc)	$v_A$ ( $\text{km s}^{-1}$ )	$\delta$
1	2.7	2	35.0	0.33
2	5.3	4	33.5	0.33
3	9.4	10	28.6	0.33

ulation of MSPs (Yuan & Zhang 2014) are also shown. The results show that there is indeed a VHE component, mainly from the ICS off the starlight, if the injection energies of the  $e^\pm$  are high enough. For the monochromatic injection case with  $E_{\text{inj}} = 20$  GeV, the ICS emission falls in the same energy window of the current GC excess. It may contribute partially to the observed signal. However, the spatial morphology of this ICS component should be different from the direct  $\gamma$ -ray emission from MSPs (see Fig. 4). For  $E_{\text{inj}} = 200$  GeV case, if  $f_{e^\pm} = 0.9$  the ICS emission will exceed the Fermi-LAT data

above several GeV. It may indicate that the  $e^\pm$  efficiency may not be as high as  $\sim 1$ , or such a high energy tail is missed in the Fermi-LAT data analysis because of the different morphology. There is a bump of the  $\gamma$ -ray emission at  $10 - 200$  GeV corresponding to  $E_{\text{inj}} = 200$  GeV, and might be detectable by future VHE observations. For the power-law injection model, the spectrum of the VHE component is shallower and can probably extend to much higher energies.

In order to have a rough idea of the detectability of this VHE emission, we compare it with the HESS detected diffuse ridge emission, integrated in the region  $|l| < 0^\circ.8$ ,  $|b| < 0^\circ.3$  in Figs. 1 and 2 (Aharonian et al. 2006). The VHE component from the MSPs could be comparable or even brighter than the ridge emission, although it is more extended. Given the much better sensitivity of the future VHE experiments such as CTA, it should be possible to detect such a bright source (Acharya et al. 2013).

Due to the extension of the emission, the nearly isotropic electron background will contaminate the detection. The spectrum of the total  $e^\pm$  based on AMS-02 (Aguilar et al. 2014) and HESS (Aharonian et al. 2008) measurements are also shown by the gray line in Figs. 1 and 2. We can see that

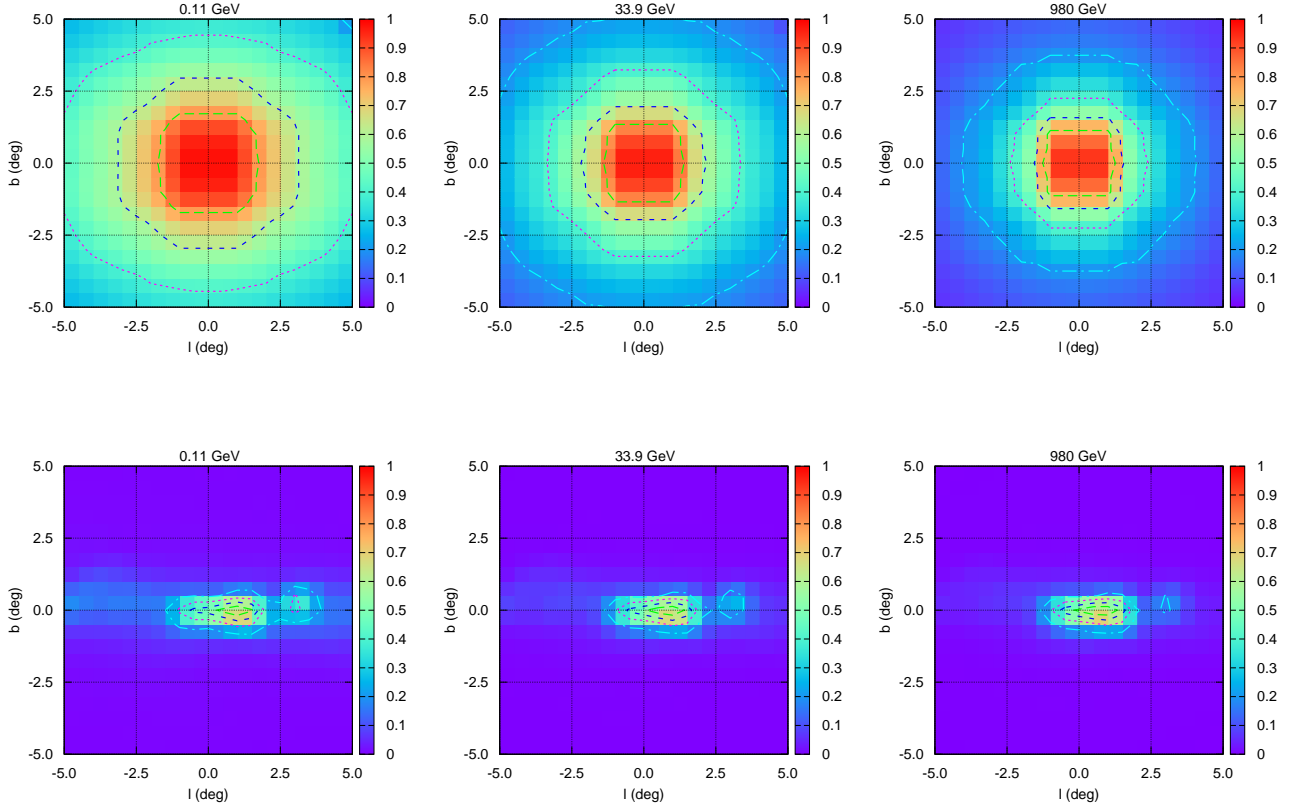


FIG. 3.— Skymaps of the ICS (top) and bremsstrahlung (bottom) emission in the central  $10^\circ \times 10^\circ$  region around the GC. Contours show the flux levels 0.8, 0.6, 0.4 and 0.2 of the peak value from inside to outside. The injection model is the exponential cutoff power-law one in Table 1, and the propagation parameters are the second group in Table 2. For each panel we normalize the maximum flux to 1 to show the relative image. Three different energies, 0.11, 33.9 and 980 GeV, are shown from left to right.

for the power-law injection scenario with a large value of  $f_{e^\pm}$ , the ICS emission may exceed the electron background for energies higher than several TeV (the left panel of Fig. 2). However, in general the electron background is much higher than the expected  $\gamma$ -ray signal. Therefore, the spatial morphology may be necessary to subtract the electron background.

Fig. 3 shows the morphology of the ICS (top panels) and bremsstrahlung (bottom panels) emission, for the power-law injection scenario. From left to right we show the results at 0.11, 33.9 and 980 GeV, respectively. The ICS emission is almost symmetric around the GC, and shows a decrease beyond  $\sim 2^\circ$ . The morphology becomes more concentrated with the increase of energy, which is expected due to the more significant cooling of higher energy  $e^\pm$ . The morphological study of the Fermi-LAT  $\gamma$ -ray excess shows that the signal is pretty symmetric with the axis ratio departing from unity less than 20% (Daylan et al. 2014). However, the current Fermi-LAT data may not be able to exclude a slightly asymmetric morphology. The CTA, on the other hand, may determine more precisely the morphology of this signal if the flux is high. We should keep in mind that there are more complexities about the very detailed morphology of the ICS emission, caused by the particle diffusion and the distribution of the background radiation field. The bremsstrahlung emission is strongly correlated with the gas distribution, and is more concentrated in the Galactic plane. It may be contaminated by the diffuse  $\gamma$ -ray background from the Galactic CRs. As we

have seen before, the ICS emission will generally dominate the bremsstrahlung one. Therefore, the nearly symmetric ICS component of the VHE emission is an important expectation of the MSP model to explain the Fermi-LAT GC excess. The morphology of the ICS emission will be crucial to eliminate the electron background.

As a comparison, we show in Fig. 4 the skymap of the ICS emission integrated in 1 – 10 GeV range, and the contours of the observed Fermi-LAT GeV  $\gamma$ -ray excess (Fig. 4 of Gordon & Macías 2013). The model parameters to calculate the ICS emission are the same as those in Fig. 3, and the flux levels of the contours of Fermi-LAT data are 0.8, 0.6, 0.4 and 0.2 from inside to outside. The result does show that the direct emission from the MSPs is much more concentrated than the ICS emission.

Finally we give the surface brightness distribution of the ICS emission above 0.1 TeV in Fig. 5. The propagation parameters are the second ones in Table 2. We adopt the efficiency  $f_{e^\pm} = 0.9$  for both the monochromatic and the power-law injection scenarios, and  $E_{\text{inj}} = 200$  GeV for the monochromatic injection scenario. The surface brightness decreases with the increase of  $\theta$ , angle away from the GC. The rough behavior beyond  $1^\circ$  is  $\sim \theta^{-0.9}$ , which is shallower than that of the Fermi-LAT excess. It is mainly due to the diffusion of the  $e^\pm$ . The HESS observation of the GC ridge emission, calculated from the fitting spectrum  $1.73 \times 10^{-8} (E/\text{TeV})^{-2.29} \text{ TeV}^{-1} \text{ cm}^{-2} \text{ s}^{-1} \text{ sr}^{-1}$  (Aharonian et al. 2006), is shown by the

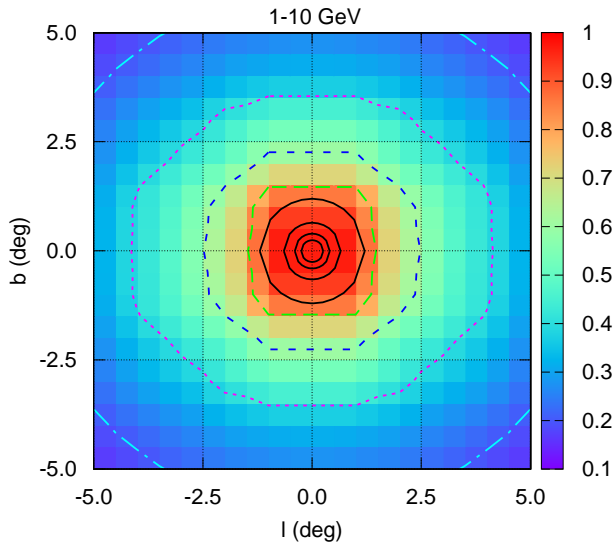


FIG. 4.— Skymap of the ICS emission integrated in 1–10 GeV range. Other parameters are the same as Fig. 3. The solid (black) lines are the contours with flux levels 0.8, 0.6, 0.4 and 0.2 of the peak value (integrated within  $0^\circ.1$ ) from inside to outside, as shown in the Fermi-LAT data of the GeV  $\gamma$ -ray excess (Gordon & Macías 2013).

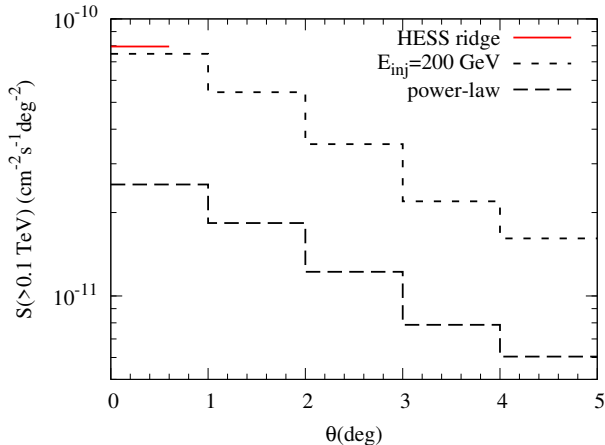


FIG. 5.— Surface brightness distribution of the ICS component from the wind  $e^\pm$  of the MSPs. The second setting of propagation parameters in Table 2 is adopted. Here  $f_{e^\pm} = 0.9$  is assumed, and for the monochromatic injection scenario we adopt  $E_{\text{inj}} = 200$  GeV. The HESS observation of the diffuse emission from the GC ridge is also plotted (Aharonian et al. 2006).

short-dashed line. The ICS emission seems to be fainter than the ridge emission. Since the sensitivity of CTA will be better by order of magnitude than HESS, it is possible for CTA to identify such a VHE  $\gamma$ -ray component.

#### 4. CONCLUSION AND DISCUSSION

The recent discovery of the GeV  $\gamma$ -ray excess from the GC in Fermi-LAT data has triggered extensive discussions of the DM origin or astrophysical origins such as MSPs. It is very essential to investigate the possible effects for future observations which may test different models. For the MSP scenario, it is expected that the wind  $e^\pm$ , with very high Lorentz fac-

tor ( $\sim 10^6$ ), will carry most of the pulsar spin-down energy, and may diffuse and radiate in the vicinity of the GC. The ICS and bremsstrahlung emission from those wind  $e^\pm$  may be detectable by the VHE  $\gamma$ -ray experiments such as CTA.

We find that there could be a bright VHE component from the wind  $e^\pm$ , mainly from the ICS off the interstellar radiation field, for a variety of model parameters. This ICS emission is nearly spherically symmetric within several degrees of the GC. The spectrum depends on the assumption of the  $e^\pm$  injection, and can likely extend to higher than 100 GeV for reasonable model parameters. The ICS emission has larger total flux than the Galactic ridge emission observed by HESS (Aharonian et al. 2006), although the former is more extended than the latter, and may be detectable with CTA. The detection of a VHE counterpart of the GeV  $\gamma$ -ray excess will provide a strong support of the MSP (or other similar astrophysical) scenario to explain the GeV  $\gamma$ -ray excess compared with the DM annihilation scenario.

The detailed detectability of the VHE source with CTA relies on the detector performance and background rejection technique for extended source analysis. These are interesting future works. Through a rough comparison with the HESS data of the GC ridge and the improvement of the sensitivity of CTA compared with HESS, it should be promising for CTA to detect such VHE emission.

We should note that the globular clusters, which are thought to be rich of MSPs, have been shown to be a class of  $\gamma$ -ray sources by Fermi-LAT (Abdo et al. 2010). Similar to the scenario discussed in this work, the VHE  $\gamma$ -ray emission from the ICS of the wind  $e^\pm$  is expected from the globular clusters (Bednarek & Sitarek 2007; Venter et al. 2009; Cheng et al. 2010). HESS has discovered the VHE  $\gamma$ -ray emission from the direction of globular cluster Terzan 5 (Abramowski et al. 2011), and set an upper limit for 47 Tucanae (Aharonian et al. 2009). The detectability of globular clusters with CTA has been investigated in detail in de Oña-Wilhelmi et al. (2013). Here we just check the consistency of the model prediction with the current observations. We take the power-law model as an illustration since the threshold energies of the HESS observations are relatively high (a few hundred GeV). Furthermore we adopt  $f_{e^\pm} = 0.9$  to give a maximum estimate. Assuming the ratio between the ICS component and the direct emission from MSPs for the globular clusters is the same as the GC excess discussed in this work, we find that the predicted VHE  $\gamma$ -ray flux is  $I(> 440 \text{ GeV}) \approx 2.9 \times 10^{-12} \text{ cm}^{-2} \text{ s}^{-1}$  for Terzan 5, and  $I(> 800 \text{ GeV}) \approx 4.4 \times 10^{-13} \text{ cm}^{-2} \text{ s}^{-1}$  for 47 Tucanae, based on the Fermi-LAT fluxes (Abdo et al. 2010). As a comparison, the HESS observations give  $I(> 440 \text{ GeV}) = (1.2 \pm 0.3) \times 10^{-12} \text{ cm}^{-2} \text{ s}^{-1}$  for Terzan 5 (Abramowski et al. 2011), and  $I(> 800 \text{ GeV}) < 6.7 \times 10^{-13} \text{ cm}^{-2} \text{ s}^{-1}$  for 47 Tucanae (Aharonian et al. 2009). The expectation of the VHE flux for Terzan 5 seems to be larger by a factor of  $\sim 2$  than the HESS observation. It may indicate that  $f_{e^\pm}$  should not be as high as  $\sim 1$ . However, we note that there are other uncertainties which also affect the prediction of the VHE fluxes, such as the magnetic field inside the clusters, the injection spectrum and diffusion of electrons (Bednarek & Sitarek 2007).

Another counterpart to the GeV  $\gamma$ -ray excess is obviously the radio MSPs. The Square Kilometre Array (SKA) will provide a complete census of pulsars in the Galaxy (Cordes et al. 2004; Smits et al. 2009) and complement the CTA observations.

*Note:* — When this work is at the final stage, we are aware of a similar work arXiv:1411.2980 (Petrovic et al. 2014)

which discussed the ICS emission from the MSPs.

We appreciate the anonymous referee for helpful suggestions on this paper. We thank M. Hayashida, D. Hooper, S. Kisaka, K. Kohri, T. Saito, H. Takami and B. Zhang for useful

comments. This work was initiated during Q.Y.'s stay in KEK as a Short-Term Invited Fellow. This work is supported by KAKENHI 24000004, 24103006, 26287051 and 26247042 (K.I.).

## REFERENCES

- Abazajian, K. N. 2011, *J. Cosmol. Astropart. Phys.*, 3, 10  
 Abazajian, K. N., Canac, N., Horiuchi, S., & Kaplinghat, M. 2014a, *Phys. Rev. D*, 90, 023526  
 Abazajian, K. N., Canac, N., Horiuchi, S., Kaplinghat, M., & Kwa, A. 2014b, *ArXiv e-prints*:1410.6168  
 Abazajian, K. N., & Kaplinghat, M. 2012, *Phys. Rev. D*, 86, 083511  
 Abdo, A. A., et al. 2010, *A&A*, 524, A75  
 Abdo, A. A., et al. 2013, *ApJS*, 208, 17  
 Abramowski, A., et al. 2011, *A&A*, 531, L18  
 Acharya, B. S., et al. 2013, *Astroparticle Physics*, 43, 3  
 Ackermann, M., et al. 2012, *ApJ*, 761, 91  
 Ackermann, M., et al. 2014, *ApJ*, 793, 64  
 Aguilar, M., et al. 2014, *Physical Review Letters*, 113, 121102  
 Aharonian, F., Khangulyan, D., & Malyshev, D. 2012, *A&A*, 547, A114  
 Aharonian, F., et al. 2004, *A&A*, 425, L13  
 Aharonian, F., et al. 2006, *Nature*, 439, 695  
 Aharonian, F., et al. 2008, *Phys. Rev. Lett.*, 101, 261104  
 Aharonian, F., et al. 2009, *A&A*, 499, 273  
 Bednarek, W., & Sitarek, J. 2007, *MNRAS*, 377, 920  
 Bednarek, W., & Sobczak, T. 2013, *MNRAS*, 435, L14  
 Boyarsky, A., Malyshev, D., & Ruchayskiy, O. 2011, *Physics Letters B*, 705, 165  
 Bringmann, T., Vollmann, M., & Weniger, C. 2014, *ArXiv e-prints*:1406.6027  
 Calore, F., Cholis, I., & Weniger, C. 2014a, *ArXiv e-prints*:1409.0042  
 Calore, F., Di Mauro, M., & Donato, F. 2014b, *ApJ*, 796, 14  
 Carlson, E., & Profumo, S. 2014, *Phys. Rev. D*, 90, 023015  
 Cheng, K. S., Chernyshov, D. O., Dogiel, V. A., Hui, C. Y., & Kong, A. K. H. 2010, *ApJ*, 723, 1219  
 Cheng, K. S., Taam, R. E., & Wang, W. 2006, *ApJ*, 641, 427  
 Chernyakova, M., Malyshev, D., Aharonian, F. A., Crocker, R. M., & Jones, D. I. 2011, *ApJ*, 726, 60  
 Cholis, I., Hooper, D., & Linden, T. 2014, *ArXiv e-prints*:1407.5625  
 Cirelli, M., Gaggero, D., Giesen, G., Taoso, M., & Urbano, A. 2014, *ArXiv e-prints*:1407.2173  
 Cordes, J. M., Kramer, M., Lazio, T. J. W., Stappers, B. W., Backer, D. C., & Johnston, S. 2004, *New Astron. Rev.*, 48, 1413  
 Crocker, R. M. 2012, *MNRAS*, 423, 3512  
 Crocker, R. M., Jones, D. I., Aharonian, F., Law, C. J., Melia, F., Oka, T., & Ott, J. 2011, *MNRAS*, 413, 763  
 Daylan, T., Finkbeiner, D. P., Hooper, D., Linden, T., Portillo, S. K. N., Rodd, N. L., & Slatyer, T. R. 2014, *ArXiv e-prints*:1402.6703  
 de Oña-Wilhelmi, E., et al. 2013, *Astroparticle Physics*, 43, 287  
 Dobler, G., Finkbeiner, D. P., Cholis, I., Slatyer, T., & Weiner, N. 2010, *ApJ*, 717, 825  
 Fermi-LAT collaboration. 2014, in *Fifth International Fermi Symposium* ([http://fermi.gsfc.nasa.gov/science/mtgs/symposia/2014/program/08\\_Murgia.pdf](http://fermi.gsfc.nasa.gov/science/mtgs/symposia/2014/program/08_Murgia.pdf))  
 Goldreich, P., & Julian, W. H. 1969, *ApJ*, 157, 869  
 Goodenough, L., & Hooper, D. 2009, *ArXiv e-prints*:0910.2998  
 Gordon, C., & Macías, O. 2013, *Phys. Rev. D*, 88, 083521  
 Hagiwara, K., Mukhopadhyay, S., & Nakamura, J. 2014, *Phys. Rev. D*, 89, 015023  
 Hooper, D., Cholis, I., Linden, T., Siegal-Gaskins, J. M., & Slatyer, T. R. 2013, *Phys. Rev. D*, 88, 083009  
 Hooper, D., & Goodenough, L. 2011, *Physics Letters B*, 697, 412  
 Hooper, D., Linden, T., & Mertsch, P. 2014, *ArXiv e-prints*:1410.1527  
 Hooper, D., & Slatyer, T. R. 2013, *Physics of the Dark Universe*, 2, 118  
 Huang, W.-C., Urbano, A., & Xue, W. 2013, *ArXiv e-prints*:1307.6862  
 Jin, H.-B., Wu, Y.-L., & Zhou, Y.-F. 2014, *ArXiv e-prints*:1410.0171  
 Kashiwara, K., Ioka, K., & Kawanaka, N. 2011, *Phys. Rev. D*, 83, 023002  
 Kennel, C. F., & Coroniti, F. V. 1984a, *ApJ*, 283, 694  
 Kennel, C. F., & Coroniti, F. V. 1984b, *ApJ*, 283, 710  
 Kisaka, S., & Kawanaka, N. 2012, *MNRAS*, 421, 3543  
 Kosack, K., et al. 2004, *ApJ*, 608, L97  
 Lacroix, T., Boehm, C., & Silk, J. 2014, *Phys. Rev. D*, 90, 043508  
 Macías, O., & Gordon, C. 2014, *Phys. Rev. D*, 89, 063515  
 Mirabal, N. 2013, *MNRAS*, 436, 2461  
 Moskalenko, I. V., Porter, T. A., & Strong, A. W. 2006, *ApJ*, 640, L155  
 Moskalenko, I. V., & Strong, A. W. 1998, *ApJ*, 493, 694  
 Navarro, J. F., Frenk, C. S., & White, S. D. M. 1997, *ApJ*, 490, 493  
 Petrović, J., Dario Serpico, P., & Zaharijaš, G. 2014, *J. Cosmol. Astropart. Phys.*, 10, 52  
 Petrović, J., Serpico, D. P., & Zaharijas, G. 2014, *ArXiv e-prints*:1411.2980  
 Rees, M. J., & Gunn, J. E. 1974, *MNRAS*, 167, 1  
 Revnivtsev, M., Lutovinov, A., Churazov, E., Sazonov, S., Gilfanov, M., Grebenev, S., & Sunyaev, R. 2008, *A&A*, 491, 209  
 Smits, R., Kramer, M., Stappers, B., Lorimer, D. R., Cordes, J., & Faulkner, A. 2009, *A&A*, 493, 1161  
 Strong, A. W., & Moskalenko, I. V. 1998, *ApJ*, 509, 212  
 Su, M., & Finkbeiner, D. P. 2012, *ApJ*, 753, 61  
 Su, M., Slatyer, T. R., & Finkbeiner, D. P. 2010, *ApJ*, 724, 1044  
 Trotta, R., Jóhannesson, G., Moskalenko, I. V., Porter, T. A., Ruiz de Austri, R., & Strong, A. W. 2011, *ApJ*, 729, 106  
 Venter, C., De Jager, O. C., & Clapson, A.-C. 2009, *ApJ*, 696, L52  
 Vitale, V., Morselli, A., & for the Fermi/LAT Collaboration. 2009, *ArXiv e-prints*:0912.3828  
 Wang, W., Jiang, Z. J., & Cheng, K. S. 2005, *MNRAS*, 358, 263  
 Yang, R.-z., Aharonian, F., & Crocker, R. 2014, *A&A*, 567, A19  
 Yuan, Q., & Zhang, B. 2014, *JHEAp*, 3, 1, *ArXiv e-prints*:1404.2318  
 Yusef-Zadeh, F., et al. 2013, *ApJ*, 762, 33  
 Zhao, H. 1996, *MNRAS*, 278, 488  
 Zhou, B., Liang, Y.-F., Huang, X., Li, X., Fan, Y.-Z., Feng, L., & Chang, J. 2014, *ArXiv e-prints*:1406.6948